https://dx.doi.org/10.1016/j.jpowsour.2022.231373

New interconnector designs for electrical performance enhancement of solid oxide fuel cells: a 3D modelling study

Meiting Guo, Qijiao He, Chun Cheng, Dongqi Zhao, Meng Ni*

Department of Building and Real Estate, Research Institute for Sustainable Urban Development (RISUD) and Research Institute for Smart Energy (RISE), The Hong Kong Polytechnic University, Hung Hom, Kowloon, Hong Kong, China

Abstract

Interconnector (IC) is a critical component of solid oxide fuel cell (SOFC) stack for current collection and gas distribution. However, the commonly used IC design causes low average SOFC stack performance due to the highly uneven distribution of gas (especially O_2) in the porous electrodes and the contact resistance between IC and electrode. In this study, several unconventional IC designs are proposed and studied numerically by 3D multi-physics modeling. Compared with the traditional straight channel-based IC design, the new IC design can achieve more uniform distribution of O_2 in the cathode of SOFC. As a result, the peak power density of SOFC can be improved by up to 27.86%. The performance improvement can be attributed to the discrete distribution of ribs, the reduction of rib size, and the spatial layout arrangement of discrete ribs, which may shorten gas diffusion path, current collection path, or both. It is also found that the performance degradation caused by IC oxidation is highly related to the contact area between IC and electrode. In addition, the increased parasitic power loss induced by the newly designed IC is less than 0.1% of the increased electric power, so it can be neglected.

*Corresponding author: meng.ni@polyu.edu.hk ; Tel: 852-27664152

Keywords: Multi-physics models; Electrical power; Oxygen concentration; Contact area; Contact resistance; Performance degradation.

1. Introduction

Solid oxide fuel cell (SOFC) is a promising power generation device with the advantages of high energy conversion efficiency, fuel flexibility, free of noble metal catalyst and low pollution. The scalability of SOFC enables its wide applications in various fields, e.g., portable power, transportation power, distributed power station, and large-scale stationary electric power plant.

Among SOFCs of various shapes and support types, the planar anode-supported SOFC is most popular due to its compactness and larger volume power density. To deliver a high voltage and high power output, multiple cells need to be connected in series by interconnector (IC) to assemble an SOFC stack. A repeating unit of SOFC stack consists of IC, gas channels, sealant and PEN (Positive electrode-Electrolyte-Negative electrode) components. Among all the constituent components, IC shoulders the functions of gas distribution, current collection, cells connection and mechanical support, which are of great significance for power output of an SOFC stack [1]. However, even for popular planar SOFC [2], the SOFC stack performance is significantly lower than that of an SOFC single cell due to uneven gas distribution and additional ohmic loss at the IC-electrode contacts [3]. Even worse, the performance of SOFC stack could decrease over time due to the oxidation of metal alloy-based IC [4], which can significantly increase the contact resistance at the IC-electrode interfaces [5].

The traditional IC consists of multiple straight parallel channels separated by rectangular solid ribs as depicted in Fig. 1a. This type of IC is widely used due to the compactness and easier fabrication [6]. When the rib size is large, current collection is easy, but the O_2 diffusion under the rib becomes difficult, which results in low local performance of SOFC under the rib.

Conversely, a small rib size facilitates O_2 diffusion under the rib, but the current collection becomes difficult. Thus, there is a tradeoff between rib and channel width or area during the 1D or 2D IC optimization process, which is inherently determined by the competition relationship between concentration loss and ohmic loss. During past years, extensive research has been conducted on rib size optimization. In 2003, Lin et al [7] developed a phenomenological model for concentration polarization and deduced an analytical expression to estimate the rib effects on concentration polarization of anode-supported SOFC, which provided an easy-to-use guidance on optimizing the rib-channel layout. In 2006, Jeon et al. [8] developed a microstructural model and examined the influence of rib width, pitch width and the electrode-IC contact area specific resistance (ASR) on stack performance. The parameters of the reference cell were either from the experimental SOFC button cell directly or obtained by fitting experimental I-V curve. Based on the reference cell, the particle radius and thickness of cathode were optimized, therefore constituting the optimal cell. It revealed that the optimal rib ratio (rib width/pitch width) was in the range of 0.4-0.6 for the reference cell, and the optimal rib ratio of the optimized cell was around 0.5–0.7 for the practical ranges of the pitch width and the intrinsic contact resistance. Later, based on the isothermal field, the design optimization of rib width of solid oxide fuel cell by numerical methods was conducted subsequently. Kong et al [9] and Liu et al [10] optimized the rib width of SOFC, and the result indicated that the optimal rib ratio was in the range of 0.4-0.6 when ASR was 0.05 Ω cm^2. Besides, the optimal rib ratio could increase with ASR between electrode and IC. However, except for the simplified temperature field, all the research work above were based on the traditional straight rib-channel IC configuration and the design optimization of rib is limited only in the width direction, which cannot solve the problem induced inherently by the continuous rectangular rib-channel configuration. As an example, for conventional SOFC IC with rib ratio 0.375 [11] and 0.5 [12], the O_2 concentration under the rib was quite low, even

the rib ratio was close to or well in the reported optimal rib ratio range [8, 10]. Hence, conducting new IC design to enhance oxygen transfer in cathode of SOFC needs to be moved forward.

In recent years, many new flow fields with various shapes have been proposed for proton exchange membrane fuel cells (PEMFCs) to address the critical issue of heat and water management, e.g., metal-foam [13], honeycomb [14], fishbone [15], spiral [16] and tree-like [17] flow field. However, the results and conclusions obtained from PEMFCs may not be applicable to SOFCs due to the significant differences between SOFC and PEMFC. In low-temperature PEMFC, the water is liquid and the transport in cathode channel is a two-phase flow problem. In addition, the thick gas diffusion layer (GDL) in PEMFC can ensure more uniform O_2 distribution in the PEMFC. For comparison, the SOFC cathode is usually thin, which may result in poor O_2 distribution uniformity. Thus, it is highly demanded to study and evaluate new IC designs for SOFC stacks. However, only a few works have reported new IC designs for SOFC in the past decades. Gao et al [18] conducted the optimization of cylindrical ribs of both anode-supported and cathode-supported SOFC with isothermal field assumption. Kong et al [19] proposed an X-type IC to increase the power density by 14.25% compared with the traditional IC design. Fu et al [20] studied the performance of SOFC by using a beam and slot IC both numerically and experimentally, the electrical performance could be increased by more than 13% at different working temperatures. Bhattacharya [21] reported the performance characteristics of SOFC with straight and serpentine channel geometries. The SOFC with serpentine flow field showed remarkably more uniform distribution of ionic current density, significantly higher power output and fuel utilization compared to that of straight channel design. However, the higher pressure drop loss by the serpentine flow filed caused additional power consumption of SOFC system. The shape of the IC ribs is only one factor affecting the performance of SOFC, and the layout of ribs and the contact area between electrode and IC

may also play significant roles in electrical performance output. The research about IC design of SOFC is still scarce. Besides, there are few systematical studies on comparative analysis of output performance of SOFC with different IC geometries, rib layouts, contact area and contact resistance. Furthermore, the effect of new IC design on performance degradation of SOFC has not been studied. Therefore, the effect of IC design on the performance of SOFC needs to be further carried out.

In this study, several unconventional IC designs are proposed to enhance the electrochemical performance and power output. The physical field distribution and electrical performance of a repeating SOFC stack unit with different IC designs are comparatively and systematically studied. The size of ribs, layout of ribs, contact area, and contact resistance between electrode and IC are all taken into consideration to better evaluate the output performance of SOFC with newly designed ICs, which have not been conducted before. The effect of IC design on species distribution, electric power, peak power density and pressure loss are all investigated. It is found that the properly designed IC can not only improve the electrical performance but also could keep higher power output during long-term operation process. Besides, IC design with less contact area may degrade more seriously with the increased oxidation of metal IC. However, the effects of the IC design on the mechanical strength, especially thermal stress are not include in the present study. We focus on the IC design at the cathode side without changing the anode side due to more uniform H_2 distribution at the anode side. Such a design may cause unbalanced compression in SOFC stack fabrication. This will be our future work.

2. Method and models

As the low O_2 concentration under the rib limits the SOFC stack performance, new IC configurations are thus proposed to enhance oxygen transfer. Eight different IC designs are

comparatively studied to better illustrate the influence of IC design on electrical performance of SOFC stack, which are schematically displayed in Fig. 1 and descriptively listed in Table 1. Except for the details of IC size, the corresponding ratios of IC/electrode contact area to the total active electrode surface area are also listed in Table 1. The schematic diagram of 3D SOFC with a traditional IC is displayed in Fig. 1a, in which the flow path of both fuel and air inside channels are marked by dotted arrows. Considering the ICs at anode side of the other cases are the same as that of case 1, only the cross section of ICs at cathode side are displayed in Fig. 1b-Fig. 1h. The green part denotes ribs, and the white part represents flow field. The air flow direction is denoted by arrows schematically in Fig. 1b-Fig.1 h. In addition, the flow field of all the cases studied is designed as counter-flow.

For all the cases, the active area is 1.2 cm × 1.2 cm. The heights of anode support layer (ASL), anode functional layer (AFL), electrolyte (ELE), cathode functional layer (CFL) and cathode current collection layer (CCCL) are 1 mm, 20 μm, 10 μm, 20 μm and 50 μm, respectively. The heights of ASL, AFL, ELE, CFL and CCCL are the same as those of the experiment cell [22]. To be more general, the height of ELE is set as 10 μm in this study, rather than 8 μm as that of experiment cell. The heights of channel and IC are 1 mm and 2 mm, respectively. Considering the practical fabrication difficulty and cost, the widths of ribs and channels for the base case (traditional IC design) are both 2 mm, the rib size is also restricted not less than 1 mm for all the IC designs to reduce the fabrication and machining difficulty. Based on the traditionally designed IC (case 1), only the shape, size or layout of ribs at cathode side are changed to design new IC while keep traditionally designed IC at anode side and all other geometrical parameters unchanged. To exclude the effect of total contact area between IC and electrode, all the cases except for case 6, 7, and 8 possess the same contact area, which occupies 50% of the total active area. Besides, the cases (case 6, 7, 8) with different contact

area are also compared to better reveal the potential influential factor on electric power and performance degradation of SOFC.

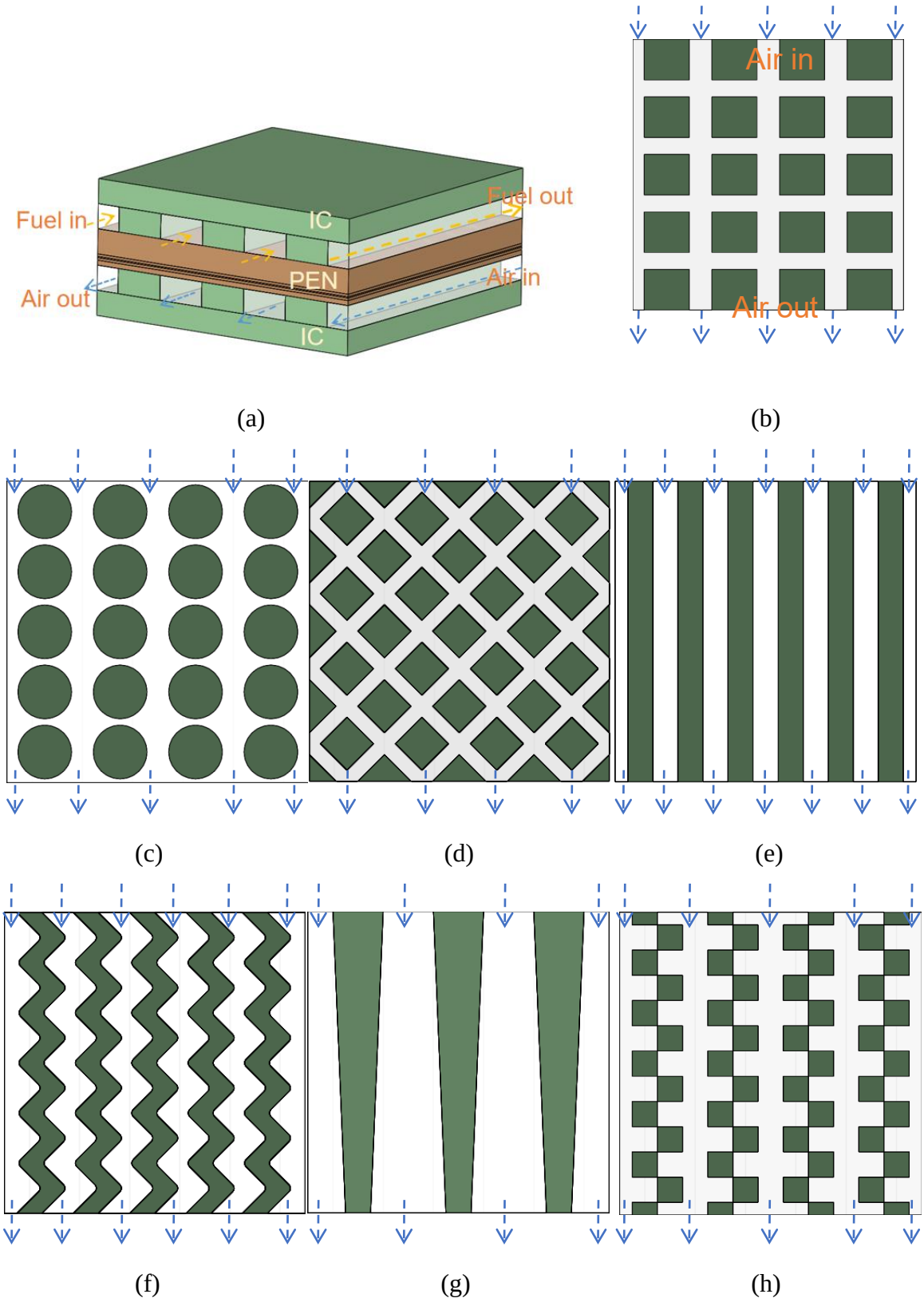

Fig. 1 (a) 3D schematic diagram of SOFC with traditional IC design; Cross section of SOFC with (b) discrete rectangular solid ribs, (c) discrete cylindrical ribs, (d) discrete rhombus ribs, (e) narrowed rib and channels, (f) wave-like ribs, (g) trapezoid ribs and (h)staggered cuboid ribs.

The materials of ASL, AFL, ELE, CFL, CCCL and IC are nickel doped-yttria stabilized zirconia (Ni-YSZ), Ni-YSZ, YSZ, strontium-doped lanthanum manganite-yttria stabilized zirconia (LSM-YSZ), LSM and Crofer 22 APU, respectively.

Table 1 Cases studied

Cases	IC geometry	Contact area/active area
Case 1	The traditionally used rectangular solid rib structure. Rib size: 2 mm ×12 mm.	50%
Case 2	Cathode adopts discrete rectangular solid ribs. Discrete rib size: 2 mm ×1.8 mm.	50%
Case 3	Cathode adopts discrete cylinder ribs. The diameter of cylinder rib: 2.12 mm.	50%
Case 4	Cathode adopts discrete rhombus ribs. Discrete rib size: 1.5 mm ×1.5 mm.	50%
Case 5	Cathode adopts 1 mm width ribs and channels. Rib size: 1 mm ×12 mm.	50%
Case 6	Cathode adopts staggered wave-like ribs. Rib width:1 mm, winding path length:16.968 mm.	41.7%
Case 7	Cathode adopts continuous trapezoidal ribs. Rib width: 2 mm (upper) and 1mm (lower), length:12 mm.	37.5%
Case 8	Cathode adopts alternatively arranged cuboid ribs. Rib size: 1 mm × 1 mm.	33.3%

The multiphysics model of SOFC includes: mass, species, momentum, energy transfer and electrochemical reaction processes. All the chemical and physical processes are strongly coupled and interact with each other. To be simplified, some reasonable assumptions are made as below:

(1) Both fuel and air are considered as ideal gas.

(2) Electronic and ionic conduction phases in the porous electrodes are continuous and homogeneous.

(3) The porous electrode is homogeneous and the pores are uniformly distributed.

(4) The local thermal equilibrium is assumed.

2.1 Mass transfer equation

Mass conservation is satisfied in the whole SOFC, although not satisfied in a separate electrode. The source term in anode and cathode are opposite of each other. The mass conservation equation can be formulated as:

$$\nabla \cdot (\varepsilon \rho \vec{u}) = S_m \tag{1}$$

where ρ, u, and S_m are density (kg m^{-3}), velocity (m s^{-1}), and the mass source term (kg m^{-3} s^{-1}). ε is the porosity of electrode, and it can be equivalent to be 1 in channel.

2.2 Species transfer models

Species conservation equation can be expressed as:

$$\nabla \cdot (\varepsilon \rho Y_i \vec{u}) = \nabla \cdot (\rho D_i \nabla Y_i + \rho D_i Y_i \frac{\nabla M_n}{M_n}) + S_i \tag{2}$$

here, $M_n = (\sum_i \frac{Y_i}{M_i})^{-1}$. Y_i and $D_{i,eff}$ are the mass fraction and effective diffusion coefficient (m^2 s^{-1}) of species i, respectively. S_i is the sink or source term (kg m^{-3} s^{-1}) of species i for

electrochemical reaction in active area. The source terms associated with electrochemical reaction are represented as:

$$S_{H_2} = -\frac{j}{2F} \tag{3}$$

$$S_{H_2O} = \frac{j}{2F} \tag{4}$$

$$S_{O_2} = -\frac{j}{4F} \tag{5}$$

The species diffusion process is modeled by Dusty-Gas model, which has been proven to be the most accurate model to simulate gas diffusion in porous electrode of SOFC [23] at present. Binary diffusion coefficient is generally used directly to model gas transfer in channels, where gas convective transfer is dominated rather than diffusion transfer. The mutual diffusion coefficient of binary molecules can be expressed as [10]:

$$D_{ij} = \frac{2.198\times T^{1.75}}{P\left(v_i^{1/3}+v_j^{1/3}\right)}\left(\frac{1}{M_i}+\frac{1}{M_j}\right)^{0.5} \tag{6}$$

where T, v_i and M_i are temperature (T), diffusion volume ($m^3\,mol^{-1}$) and molar mass ($kg\,mol^{-1}$) of species i. P is the absolute gas pressure (Pa).

In electrode, the influence of porosity (ε) and tortuosity (τ) should be considered to describe effective binary molecule diffusion coefficient.

$$D_{ij}^{eff} = \frac{\varepsilon}{\tau} D_{ij} \tag{7}$$

In electrode, molecule diffusion dominates when electrode pore is larger than molecule mean free path, while Knudsen diffusion is considered when the collision between gas molecule and pore wall becomes primary. The effective Knudsen diffusion coefficient of component i can be formulated as:

$$D_{ik}^{eff} = \frac{2\varepsilon}{3\tau} r_g \sqrt{\frac{8RT}{\pi M_i}} \tag{8}$$

here r_g is pore radius (m) and expressed as:

$$r_g = \frac{2}{3}\frac{1}{1-\varepsilon}\frac{1}{\varphi_{el}/r_{el} + \varphi_{io}/r_{io}} \tag{9}$$

here φ_{el} and φ_{io} are volume fraction of electron and ion conducting particles.

Considering both molecule diffusion and Knudsen diffusion, the effective diffusion coefficient of species *i* in electrode is expressed as [10]：

$$D_i^{eff} = \frac{D_{ij}^{eff} D_{ik}^{eff}}{D_{ij}^{eff} + x_i D_{jk}^{eff} + x_j D_{ik}^{eff}} \tag{10}$$

where x_i is the molar fraction of species *i*.

2.3 Momentum transfer model

Both fuel and air flow in channel are laminar and modeled using Navier-Stokes equations:

$$\rho(\vec{u}\cdot\nabla)\vec{u} = -\nabla\cdot PI + \nabla\cdot[\mu(\nabla\vec{u} + (\nabla\vec{u})^T)] + S_u \tag{11}$$

where μ and S_u are the dynamic viscosity (Pa·s) of mixture gas and source term (N m-3) of momentum equation, respectively. *I* is the unit vector.

The flows in the porous electrodes are governed by Brinkman equations. These equations are the combination of continuity equation (Eq.1) and momentum equation based on Darcy velocity and pressure. These equations could be expressed as follow:

$$\frac{\rho}{\varepsilon}(\vec{u}\cdot\nabla)\frac{\vec{u}}{\varepsilon} = \nabla\cdot[-P\,\mathrm{I} + \frac{\mu}{\varepsilon}(\nabla\vec{u} + (\nabla\vec{u})^T) - \frac{2}{3\varepsilon}\mu(\nabla\cdot\vec{u})\,\mathrm{I}] - (\frac{\mu}{k} + \frac{S_m}{\varepsilon^2})\vec{u} + S_u \tag{12}$$

where *k* is the permeability (m^2) of electrode.

2.4 Electrochemical reaction model

The electrochemical reactions include H_2 oxidation reaction in anode and O_2 reduction reaction (ORR) in cathode. Hydrogen transfers to three phase boundary (TPB) of anode and

electrochemically reacts with O^{2-} to produce steam and electrons. The released electrons from anode are transferred through external circuit to cathode, where they react with oxygen molecules to form O^{2-}. The two half electrochemical reactions can be expressed as:

$$H_2 + O^{2-} \rightarrow H_2O + 2e^- \text{ Anode} \tag{13}$$

$$0.5O_2 + 2e^- \rightarrow O^{2-} \text{ Cathode} \tag{14}$$

Electronic current and ionic current transfer are governed by charge conservation equations:

$$\nabla \cdot \vec{i}_{el} = \nabla \cdot (-\sigma_{el}^{eff} \nabla \phi_{el}) = \begin{cases} -j_{TPB}\lambda_{TPB,eff} & \text{Anode} \\ j_{TPB}\lambda_{TPB,eff} & \text{Cathode} \end{cases} \tag{15}$$

$$\nabla \cdot \vec{i}_{io} = \nabla \cdot (-\sigma_{io}^{eff} \nabla \phi_{io}) = \begin{cases} j_{TPB}\lambda_{TPB,eff} & \text{Anode} \\ 0 & \text{Electrolyt e} \\ -j_{TPB}\lambda_{TPB,eff} & \text{Cathode} \end{cases} \tag{16}$$

where n is the transferred electron number in unit electrochemical reaction, $\boldsymbol{i_{el}}$ and $\boldsymbol{i_{io}}$ are the electronic and ionic current density vector (A m^{-2}), respectively. ϕ_{el} and ϕ_{io} are the electronic and ionic potential (V), respectively. $\lambda_{TPB,eff}$ (m^{-1}) is the effective TPB density per unit volume. j_{TPB} is the current density at active area. α and β are charge transfer coefficients.

Nernst potential is expressed as:

$$E_{Nernst} = \frac{-\Delta G}{2F} + \frac{RT}{2F} Ln(\frac{P_{H_2,ref}}{P_{H_2O,ref}}) + \frac{RT}{4F} Ln(\frac{P_{O_2,ref}}{P_0}) \tag{17}$$

Here, ΔG is Gibbs free energy change (J mol^{-1}) of electrochemical reaction under standard condition. $P_{H2,ref}$, $P_{O2,ref}$ and $P_{H2O,ref}$ are partial pressure (Pa) of H_2, O_2 and H_2O in reference state. P_0 is the standard atmospheric pressure.

The output voltage of SOFC in operation can be expressed as:

$$V_{cell} = E_{Nernst} - \eta_{ohm} - \eta_{act} - \eta_{con} \tag{18}$$

where η_{ohm}, η_{act} and η_{con} are ohmic, activation and concentration loss. Ohmic loss is induced by electrical resistance of solid components and is calculated by ohm's law:

$$\eta_{ohm} = j \times ASR_{ohm} \tag{19}$$

where ASR_{ohm} is the total area specific resistance (Ω cm^2).

The occurrence of electrochemical reaction needs to overcome reaction activation energy barrier, which leads to irreversible polarization loss. The relationship between current density and activation loss is described by Butler-Volmer equations:

$$\begin{cases} j_{TPB,an} = j_{0,H_2} \exp(-\dfrac{E_{H_2}}{R}(\dfrac{1}{T} - \dfrac{1}{T_{ref}}))(\dfrac{P_{H_2} P_{H_2O}}{P_{H_2,ref} P_{H_2O,ref}}) \\ j_{TPB,ca} = j_{0,O_2} \exp(-\dfrac{E_{O_2}}{R}(\dfrac{1}{T} - \dfrac{1}{T_{ref}}))(\dfrac{P_{O_2}}{P_{O_2,ref}})^{0.25} \end{cases} \tag{20}$$

where $j_{0,H2}$ and $j_{0,O2}$ are the exchange current densities (A m^{-2}) of anode and cathode in the reference condition. $j_{TPB,an}$ and $j_{TPB,ca}$ are the current densities (A m^{-2}) in the active area of anode and cathode. E_{H2} and E_{O2} are the activation energies (kJ mol^{-1}) of anode and cathode electrochemical reaction, which are the energy barriers needing to be overcome by species to reach activation state.

The concentration loss is induced by species consumption and production by electrochemical reaction of an operating SOFC. The concentration losses in anode and cathode are respectively formulated as below.

$$\eta_{con,a} = \frac{RT}{2F} Ln(\frac{P_{H_2,ref} P_{H_2O}}{P_{H_2} P_{H_2O,ref}}) \tag{21}$$

$$\eta_{con,c} = \frac{RT}{4F} Ln(\frac{P_{O_2,ref}}{P_{O_2}}) \tag{22}$$

.

2.5 Energy transfer model

Heat transfer inside SOFC includes both convective heat transfer and heat conduction. The heat radiation is ignored in this study. The energy conservation equation of SOFC can be expressed as:

$$\nabla \cdot (\rho c_p \vec{u} T) = \nabla \cdot (k_{eff} \nabla T) + S_h \quad (23)$$

where S_h is heat source (W m^{-3}), including the entropy change of electrochemical reaction, activation heat and ohmic heat.

2.6 Model validation

The multiphysics model is verified by comparing the theoretical I-V curves to that of experimental data [22] at three different operating temperatures. The experimental button cell is composed of anode support layer, anode function layer, electrolyte, cathode function layer, cathode current collector layer, and the corresponding constituent materials are respectively Ni-YSZ, Ni-YSZ, YSZ, LSM-YSZ, and LSM. The corresponding thicknesses of the components mentioned above are 1 mm, 20 μm, 8 μm, 20 μm, 50 μm, respectively. The microstructural parameters of the experiment cell are listed in Table 2. The molar ratio of H_2 to H_2O provided at anode side is 0.97:0.03, while the molar ratio of O_2 to N_2 provided at cathode side is 0.21:0.79. It can be seen from Fig. 2 that the simulation results agree well with experimental data [22], which proves the validity of the multi-physics model.

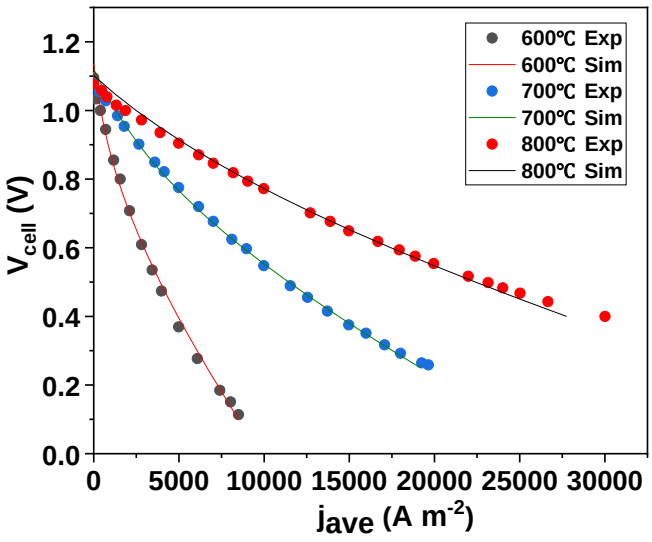

Fig. 2 Comparison of simulated and experimental I-V curve.

2.7 Grid independence test, working and boundary conditions

To avoid the effect of grid setting on accuracy of simulation result, grid independence test has been conducted for all the cases. Finally, the grids number chosen for case 1-case 8 are 67968, 83093, 89343, 85643, 67968, 101093, 113080 and 93268, respectively. It should be noted that all the cases have the same grid number setting in the height direction of components. The difference of total grid number is induced by IC with different shapes.

Table 2 Basic parameters used

Parameters	ASL	AFL	CFL	CCCL
ε	0.48	0.23	0.26	0.45
τ	3	3	3	3
φ_{el}	55%	55%	47.5%	100%
$j_{a,ref}$ (A m^{-2})		8.0E-3		
$j_{c,ref}$ (A m^{-2})			1.25E-3	
$\lambda_{TPB,eff}$ (m^{-1})		1.53E+12	2.71E+12	
a_a, β_a		1, 0.5		
a_c, β_c			0.65, 0.35	
E_{H2} (kJ mol^{-1})		120		
E_{O2} (kJ mol^{-1})			130	

All the mathematical and physical models are illustrated above. The basic geometrical, microstructural, and electrochemical parameters used are directly referred to the experimental cell [22] or obtained by fitting experimental I-V data, and the effective property parameter models used can be referred to the previous work [9, 24]. The parameters needed are listed in Table 2. More details about parameters used can be found in literature [9]. The boundary conditions are prescribed as listed in Table 3. It can be seen from Table 3 that the inlet

temperatures of both air and fuel flow are 973 K. The electric potentials at the terminate of anode and cathode ICs are open open circuit voltage (E_{ocv}) and output voltage (Vcell) 0.7 V, respectively. It's assumed the SOFC studied operates with adiabatic boundary. More details about boundary condition setting can be referred to Table 3.

To make a more reasonable comparison, for all the cases, the active area, fuel/air inlet flow rate, inlet temperature and all the other working parameters and boundary conditions are kept the same, except for the IC design at cathode side. The 3D multiphysics model, together with the boundary conditions, is solved by the finite element method. In order to avoid non-convergence, the oxygen mass fraction is set as 1E-9 when it reaches 0 or negative during the numerical iteration process.

Table 3 Boundary conditions

Boundary	Boundary conditions setting
Fuel inlet	4.66E-8 kg s^{-1} (mass flux); 97% H_2 and 3% H_2O (molar fraction); 973 K
Air inlet	1.084E-6 kg s^{-1} (mass flux); 21% O_2 and 79% N_2 (molar fraction); 973 K
Fuel/Air outlet	101325 Pa (absolute pressure); $-\vec{n}\cdot(k\nabla T)=0$; $-\vec{n}\cdot(\rho D_i^{eff}\nabla Y_i)=0$
Terminal of anode IC	$\phi_{el}=E_{ocv}$; $\frac{\partial \phi_{io}}{\partial n}=0$; Adiabatic
Terminal of cathode IC	ϕ_{el}=0.7 V; $\frac{\partial \phi_{io}}{\partial n}=0$; Adiabatic
AFL/ASL CFL/CCCL Channel/ASL Channel/CCCL	Continuous
AFL/ELE CFL/ELE	Coupled wall
Other external boundary	Electric insulation; Adiabatic

3. Results and discussion

For an anode-supported SOFC stack, the continuous straight rib-channel structure is the most widely used IC configuration. However, due to the coverage of ribs, it is difficult to convey oxygen timely to cathode region underneath ribs through horizontal oxygen diffusion, which degrades the local cell performance under the ribs, thus decreasing the overall electric power output. To solve the problem, we propose some new IC designs at cathode side with IC at anode side unchanged. Given the output voltage, the current densities are obtained and compared to elaborate the change of output performance of SOFC with different ICs.

3.1 The effect of IC design on species distribution of SOFC

Generally, H_2 concentration distributes uniformly in an anode-supported SOFC, so the concentration gradient of H_2 is not a serious issue compared to that of O_2 in SOFC. To further prove it, the standard deviations of normalized H_2 and O_2 concentration are calculated in this study and shown in Fig. 3a and Fig. 3b. It can be inferred that the distribution of H_2 concentration is far more uniform than that of O_2 concentration. The larger current density will lead to larger oxygen concentration gradient. Therefore, only the distribution of oxygen concentration of SOFC without considering the effect of ASR is studied and shown in Fig. 4.

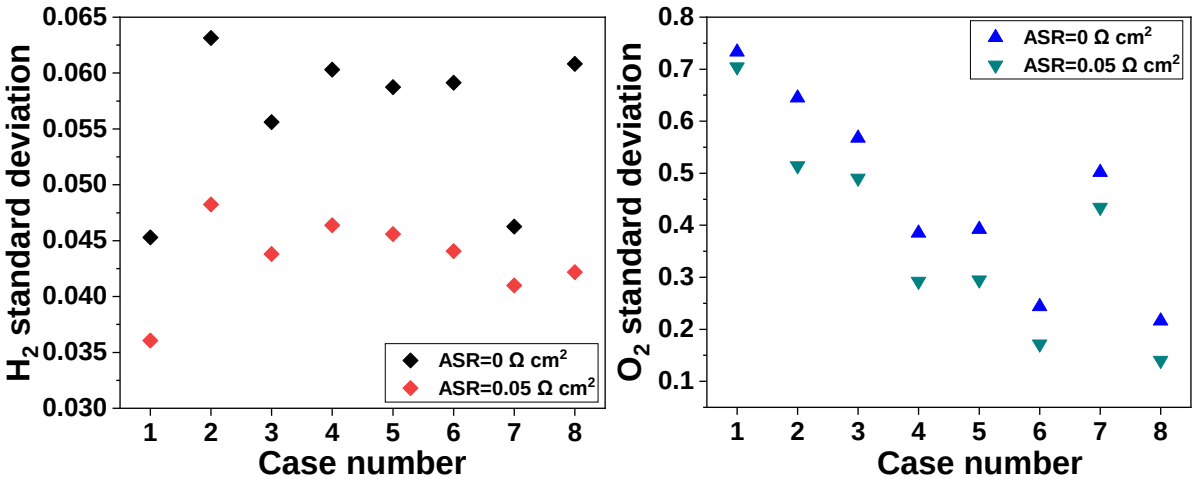

Fig. 3 The standard deviation (σ) of (a) normalized H_2 concentration and (b) normalized O_2 concentration of catalyst layer.

For an operating SOFC, oxygen is supplied from air inlet, then it flows mainly along channels toward the outlet. Perpendicular to the main flow direction, oxygen molecules diffuse into cathode, finally they participate in ORR in TPB area, leading to the concentration gradient of O_2 in SOFC. Fig. 4 shows the distribution of O_2 concentration at the cathode-electrolyte interface. To give a better visualization of distribution difference of O_2 concentration, the color legends of all the eight graphs are set as the same, in the range of 0-2.49 mol/m^3. It can be seen from Fig. 4 that IC design can greatly affect O_2 concentration distribution, and improper IC design can result in larger oxygen concentration gradient and oxygen-free zone, which limit the further improvement of electrical performance. As can be seen from Fig. 4, the minimum oxygen concentration of case 1, 2, 3, and 7 are all close to zero, and the low oxygen region occupies a considerable proportion. Even so, the low oxygen regions of case 2, 3, and 7 are all less than that of case 1. However, oxygen concentration can be more uniformly distributed by using some new IC designs in SOFC. For case 4, 5, 6 and 8, the minimum oxygen concentration is 0.15, 0.44, 0.7 and 0.78 mol m^{-3}, respectively. The oxygen concentration distribution is highly non-uniform for case 6 (Fig. 4f), as the flow field is not symmetrical, due to the different inlets/outlets of the channels at the left and right hand side. More importantly, the low oxygen region occupies a smaller proportion. It can be seen from Fig. 3b, the standard deviations of normalized O_2 concentration of these four cases are all lower than 0.4, far below than 0.73 of case 1. Consequently, with proper IC design, the uniformity of oxygen concentration distribution has been greatly improved. As the distribution of species and current density are strongly coupled together [25], it can be speculated that the design of IC will be influential on electrical performance.

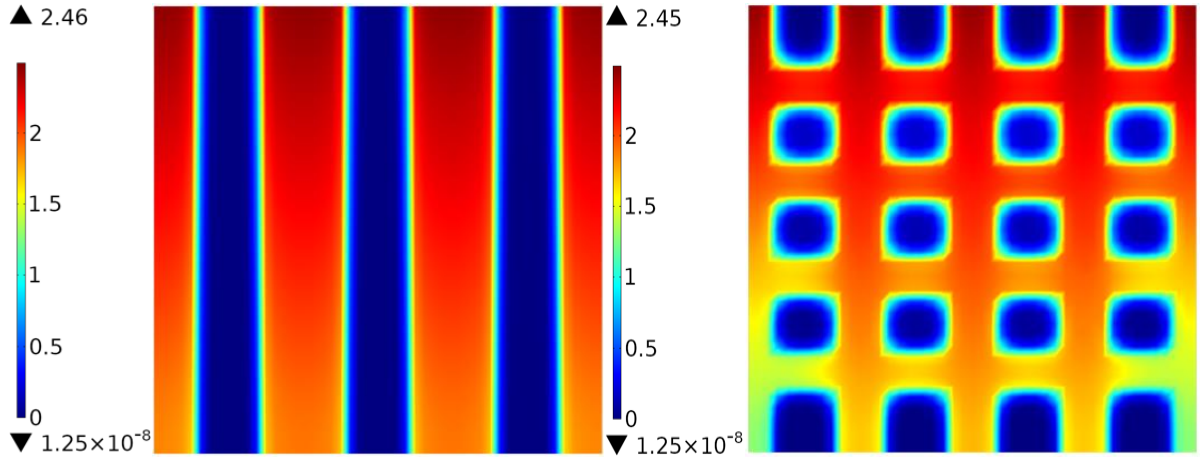
▲ 2.46
2
1.5
1
0.5
0
▼ 1.25×10^-8
▲ 2.45
2
1.5
1
0.5
0
▼ 1.25×10^-8

(a) (b)

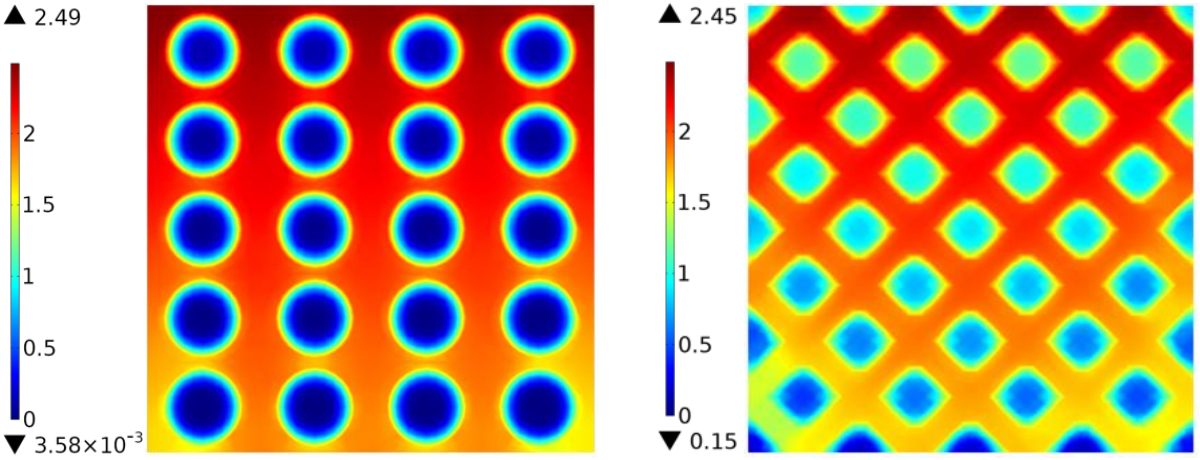
▲ 2.49
2
1.5
1
0.5
0
▼ 3.58×10^-3
▲ 2.45
2
1.5
1
0.5
0
▼ 0.15

(c) (d)

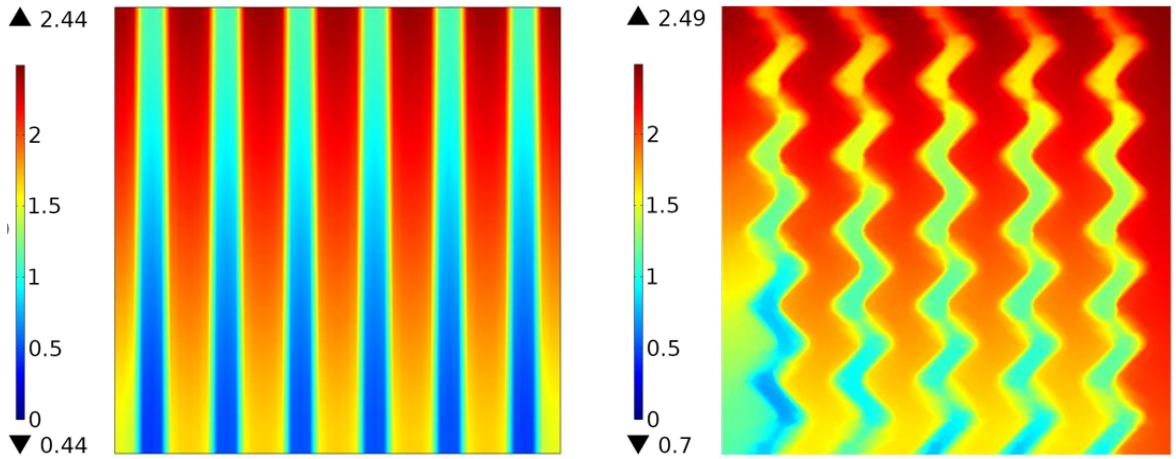
▲ 2.44
2
1.5
1
0.5
0
▼ 0.44
▲ 2.49
2
1.5
1
0.5
0
▼ 0.7

(e) (f)

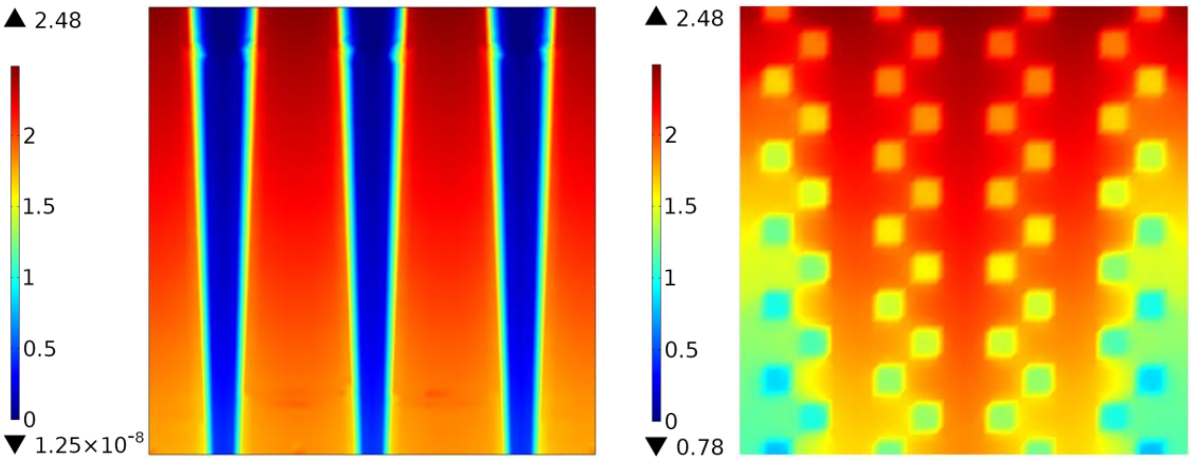

(g) (h)

Fig. 4 The distribution of oxygen concentration (mol m-3) at the cathode-electrolyte interface of case 1-case 8.

3.2 The effect of IC design on electrical performance of SOFC

The average current densities of all the cases studied are presented in Fig. 5. For case 1, case 2, and case 3, the rib sizes are kept as close as possible to make the comparison more reasonable. By comparing the average current densities of case 1, 2, and 3, it indicates that the discrete rib design can significantly improve the output performance. Compared with the base case, the electrical performance of case 2 is improved by 15.54%, while the electrical performance of case 3 is increased by 16.45%. The performance improvement by using discrete ribs is consistent with the experiment result of proton exchange membrane fuel cell [26]. By using this design feature, the oxygen transportation can be conducted mainly from horizontal and vertical directions (case 2) and multiple directions (case 3) to cathode area covered by ribs, rather than only the width direction in case 1. Besides, the air channels are connected when the continuous ribs are cut into multiple parts, which makes the oxygen transfer among channels possible. Consequently, as shown in Fig. 4a, Fig. 4b, and Fig. 4c, the oxygen concentration gradient and oxygen-depletion zone of case 2 and 3 is reduced compared to case 1, which promotes the electrochemical reaction and thus increases the current generation. Even the

electrical performance has been increased by more than 15% when using discrete ribs layout in case 2 and case 3, there still exists a considerable area with low oxygen concentration, which is unfavorable for further improving the output electrical power and the peak power density. The same feature for the first three cases is the larger rib size, e.g., the larger rib width, length and radius. Therefore, it can be inferred that the size of rib needs to be further reduced to better improve the distribution uniformity of oxygen concentration.

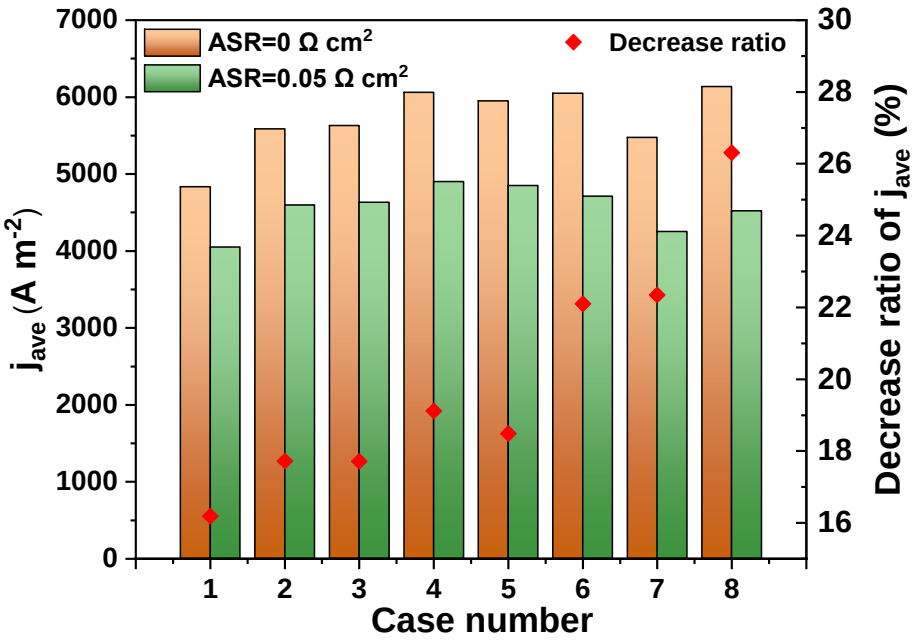

Fig. 5 The average current density (j_{ave}) and the corresponding current decrease ratio due to ASR

For case 4-case 8, we try to reduce the size of ribs when designing new ICs. As to case 4, the side length of rib is reduced to 1.5 mm, decreasing the diffusion path of oxygen from cathode under channels to cathode area under ribs, thus helping to decrease oxygen concentration gradient and increase the utilization of electrochemical reaction sites. Besides, the staggered arrangement of rhombus ribs in both width and length direction can help to drive reactant gas convectively into the gas diffusion layer and deliver reactant species directly to the TPB area. Due to the more tortuous transfer path, the residual time of gases in channels increases more significantly than that of case 2 and case 3, which can enhance oxygen

transportation to cathode, just as illustrated in literature [27]. As a result, the electrical performance of case 4 is improved by 25.37% compared to case 1, 9.83% and 8.92% higher that of case 2 and case 3. With regard to case 5, the rib width is reduced to 1 mm. The narrower rib facilitates oxygen diffusion into cathode area underneath rib, while narrower channel and continuous rib both benefit current collection. Consequently, the electrical power of case 5 is improved by 23.09% compared to that of case 1. The performance improvement by this method is consistent with the experimental result [28], which reduces lateral current collection loss by increasing the number of ribs and decreasing the size of metal mesh. In terms of case 6, the rib width is also reduced to 1 mm as in case 5, and the rib is also continuous without intervals. Besides, the shape of rib is winding as wave-like, so the residual time of gases in channels increases, which helps more oxygen to diffuse into cathode when air flow passes through channels. Consequently, the electrical performance is improved by 25.12% compared to that of case 1. For SOFC, the oxygen depletion becomes serious when air flows from inlet toward outlet. Based on this, a continuous trapezoidal rib (case 7) is proposed with 2 mm rib width at air entrance side and 1 mm rib width at air outlet side to alleviate oxygen depletion in area close to the terminal of air flow. However, the electrical performance is improved only by 13.29%, about half of that of case 4 and 5. Even though the gradually decreased rib width reduces oxygen transfer path from cathode under channels to cathode underneath ribs, it increases the lateral current collection path. Hence, balancing current collection path and gas transfer path is always desirable when conducting IC optimization. With respect to case 8, the staggered cuboid ribs are adopted to help oxygen diffusion from multiple directions into cathode area covered by ribs. Besides, the edges of ribs are reduced to 1 mm. This design can not only make the oxygen diffusion into cathode area underneath ribs more conveniently, but also increases the residue time of oxygen flow when it passes through channels. Ultimately,

the electrical performance is improved by 26.91%, outperforming the performance of all the other cases.

Notably, for case 6, 7 and 8, even the contact area ratio is only 41.7%, 37.5%, and 33.3%, the electrical performance still increases considerably. For these three cases, the lower contact area ratio means the larger channel size, which promotes oxygen diffusion directly into active area in direction perpendicular to the main flow direction. Besides, less contact area also shortens oxygen transfer path from cathode under channels to cathode under ribs. Consequently, the area of oxygen depletion decreases and the utilization of active sites increases. Even though the current collection path and the electrical resistance of IC may be increased in these cases, the benefit from these IC designs to oxygen flow distribution finally offsets these disadvantages, and further increases the current generation.

3.3 The effect of contact resistance on electrical performance of SOFC

All these aforementioned discussions are based on the assumption that there is no contact resistance between electrode and IC or there is no oxidation layer growth on IC surface. However, in SOFC, metallic alloy stainless steels will be oxidized over time under the oxidizing atmosphere to which they are exposed. And the ceramic coatings are often used to slow down the rate of oxidation [29]. The effect of current collection on electrical performance will become more and more remarkable with the operation of SOFC considering the oxidation of IC while neglecting the distortion of micro-scale morphology and particle coarsening of electrode. Hence, it is necessary to consider the influence of IC oxidation induced ASR on output performance when designing a new IC for an efficient and durable SOFC.

According to the reported results [1, 9], the ASR between electrode and IC is a critical factor limiting output performance, and it is generally less than 0.1 Ω cm^2 [30-31]. ASR equal to 0.05 Ω cm^2 is considered representative [32], so this value of ASR is considered in this study

to evaluate the performance degradation induced by IC oxidation. As shown in Fig. 5, when the contact resistance is considered, the current densities of all the cases decrease due to the increased ohmic loss. Consequently, the electrical power of all the cases decreases by 16.19%, 17.73%, 17.71%, 19.12%, 18.49%, 22.10%, 22.34% and 26.31%, respectively. As illustrated in Fig. 5, the SOFC with traditional IC design performs the least degradation. For case 2 and 3, even with the same contact area as case 1, the electrical performance is decreased by approximately 17.7%, larger than 16.19% of case 1. This may be ascribed to the locally larger collection current in IC of case 2 and 3. The performance of SOFC degrades more and more seriously with the decrease of contact area. For case 8 with the least contact area, the performance is even decreased by 26.31%. There are some reasons for this phenomenon. Firstly, the decreased contact area increases the ohmic resistance of IC, which enlarges the ohmic loss induced by current transfer in IC. Secondly, the less contact area tends to lengthen the transverse current collection path in cathode, of which the relatively lower electrical conductivity and smaller thickness may lead to larger ohmic loss. Consequently, for cases considering the effect of ASR, the electrical power of case 2-case 8 increase by 13.43%, 14.34%, 20.99%, 19.72%, 16.29%, 4.97%, 11.59% compared to that of case 1. Notably, the performance advantage of case 7 is greatly weakened.

A more comprehensive understanding can be obtained by comparing the results of SOFC with and without considering ASR. The former condition prefers design facilitating gas flow, while the latter favors IC design convenient to both current collection and gas flow. For practical condition, both the gas transfer and current collection need to be balanced. By comparative analysis, it is found that the IC design of case 1 hinders oxygen diffusion obviously, while the IC design of case 7 is not favorable for current collection. Consequently, the electrical performances of case 1 and case 7 are both relatively low. In the perspective of higher electrical power output, case 4, 5, and 6 are excellent alternatives for the two conditions,

while the performance of case 2 and case 3 can be further improved by optimizing the size of ribs and the intervals between ribs. Case 8 has obvious advantages compared to the traditionally designed SOFC for the two conditions, and it will be better alternatives when contact area is further increased. Compared to the other cases, case 7 has relatively commonplace advantage over case 1 when IC is not oxidized, while this advantage is further weakened when contact resistance is increased to 0.05 Ω cm^2.

It was reported in the previous research that the oxidation of IC is a long-term process. Tens of thousands of hours are needed for the ASR to increase to 0.05 Ω cm^2 [5]. For IC with anti-oxidation coating [5], the time needed is longer than 40000 hours, which is considered as the prerequisites for commercialization of SOFC technology [33]. Therefore, SOFC with all the newly designed IC can keep long-term operation with higher power output than the traditionally designed SOFC. In addition, the different IC designs show different superiorities over case 1 when contact resistance between IC and electrode changes.

3.4 The effect of IC design on peak power density

By varying the output voltage, the I-V and I-P curves are obtained, and the peak power densities for all the cases are acquired. As can be seen from Fig. 6a and Fig. 6c, the polarization curves of all the cases are very close when output voltage is high and output current is small, and the current density deviation between curves becomes more and more obvious with the decrease of output voltage. The advantage of the newly designed ICs becomes increasingly prominent with the increase of output current, because the issues about gas transfer and current collection become more and more urgent when SOFC operates with large current density. Accordingly, it can also be inferred that the limiting current density is also improved by the new IC design.

The benefit from newly designed IC for PPD improvement is also obvious, because the PPD lies in the relatively larger current density range as shown in Fig. 6b and Fig. 6d. The peak power densities of all the cases are shown in Fig. 6e. The PPD increase percentages of the other cases than case 1 are also displayed in Fig. 6f. As seen, for the cases without considering ASR, the PPD of the traditional SOFC is only 0.460 W cm^{-2}, far lower than that of the other cases. The PPD of case 2 and 3 are 12.74% and 16.09% higher than that of case 1, respectively. Case 4, 5, and 6 have relatively higher PPD, 26.58%, 19.68%, and 24.50% higher than that of case 1. The PPD of case 7 is 0.525 W cm^{-2}, 14.11% higher than that of case 1. The PPD of case 8 is approximately 0.589 W cm^{-2}, 27.86% higher than that of case 1. The performance of case 8 outperforms all the other cases in the perspective of peak power density when ASR is not considered.

For cases considering the effect of ASR, the PPD of case 1 is decreased to 0.361 W cm^{-2}, close to that of case 7, lower than that of the other cases. The PPD of case 2, 3, 4, 5, 6 and 8 are 14.03%, 15.42%, 25.76%, 21.37%, 20.31% and 15.03% higher than that of case 1. The PPD of case 7 is 0.378 W cm^{-2}, only 4.90% higher than that of case 1. Notably, the PPD of case 4 outperforms the other cases when ASR is considered, while case 8 behaves best when ASR is not considered. The advantages of the new IC design seem to be weakened with the growth of IC oxidation, because the relationship between concentration polarization and ohmic polarization is changed. Even so, the advantages of case 4, case 5, and case 6 are still considerable when IC is oxidized during a long time. Besides, it should be noted that there is still room to improve the output electrical performance by optimizing the interval of discrete ribs of case 2, 3, and 4, which will be studied further.

Summarily, from the perspective of peak power density, when ASR is not considered, it can be seen clearly from Fig. 6e and Fig. 6f that case 4, 5, 6, and 8 have excellent performance, and case 2, 3, and 7 also have prominent advantage. When SOFC runs for a long time and the

ASR between IC and cathode grows to 0.05 Ω cm^2, case 4 and case 5 behave better, and case 2, 3, 6, and 8 also have obvious superiority, while case 7 has only slight advantage.

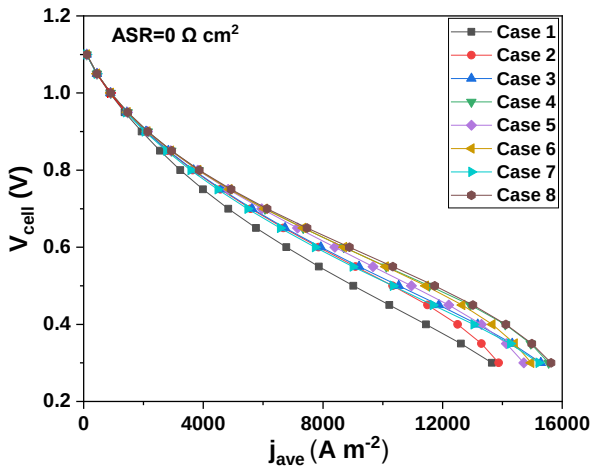

(a)

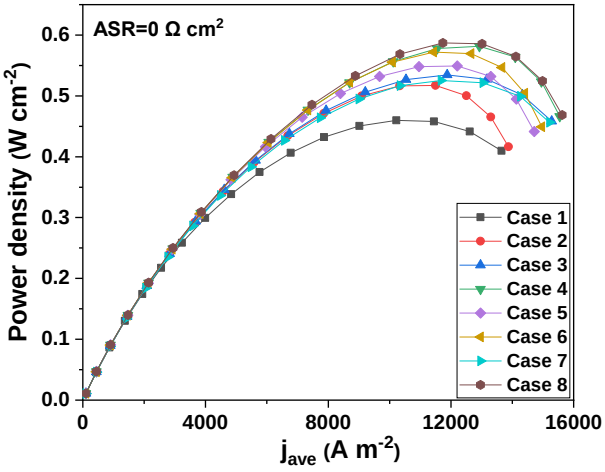

(b)

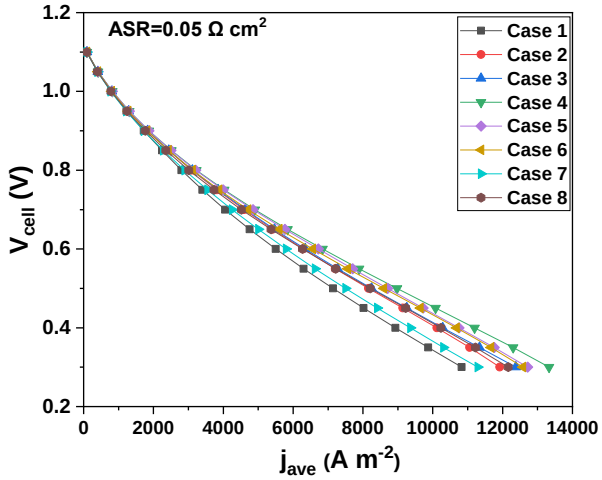

(c)

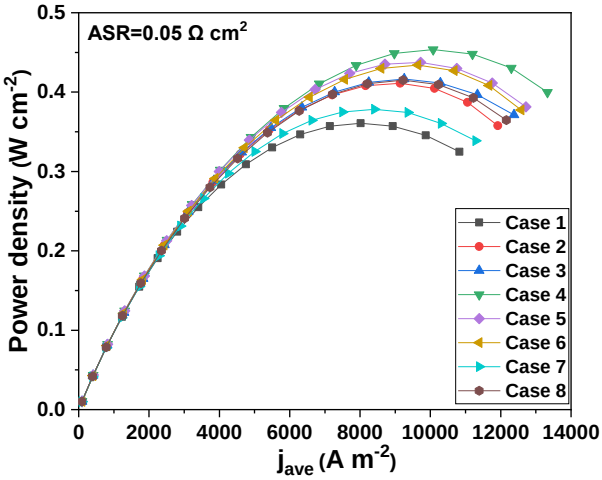

(d)

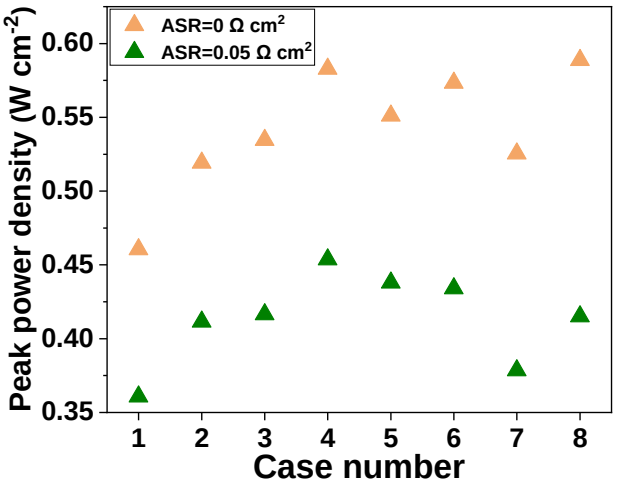

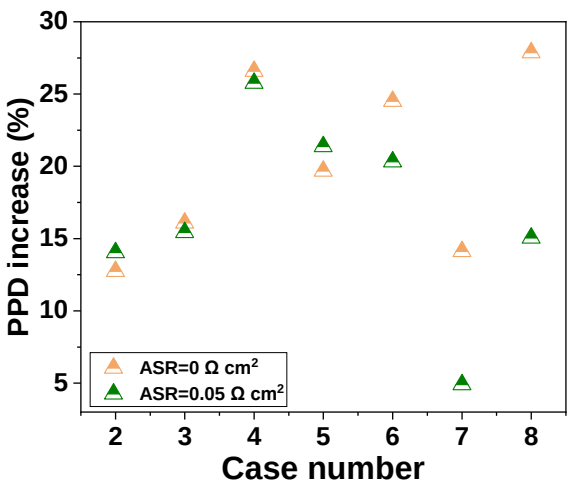

(e) (f)

Fig. 6 (a) I-V curves and (b) I-P curves without considering the effect of ASR; (c) I-V curves and (d) I-P curves considering the effect of ASR; (e) PPD of all the cases; (f) PPD increase percentage compared to case 1.

3.5 The effect of IC design on pressure drop of SOFC

Except for the electrical performance improvement, the IC or flow field design is also aimed at decreasing the pressure drop between the inlet and outlet [34] of SOFC. The relationship between the pressure drop change of gas flow along a path and the related physical quantities can be estimated by the following expression.

$$\Delta P \propto \frac{\mu u}{D^2} l$$

where pressure drop ΔP is proportional to velocity u, flow path l (m) and gas viscosity μ, while inversely proportional to the square of equivalent hydraulic diameter D (m). For all the cases studied, the inlet air mass flow rates are the same, while the inlet velocity, inlet area, gas viscosity, and realistic flow path are varied for SOFC with a different IC design. Table 4 lists the pressure difference between the air inlet (P_{in}) and air outlet (P_{out}) and the possible reasons for the pressure drop change compared to that of case 1. It should be noted that there is only slight difference of pressure drop for the case studied with and without considering the effect of ASR, therefore only the pressure drops of SOFC cases without considering ASR are listed in table 4. It can be seen from table 4 that all the cases except for case 7 have larger pressure drop than that of case 1. There are several reasons for this. Firstly, larger pressure drop is usually induced by the frictional energy loss along a longer flow path, such as serpentine flow field [35] or wave-like flow field in this study. Secondly, larger pressure is needed to drive the gas flow to pass through the narrower interval space between discrete ribs. Besides, for cases

with smaller (larger) inlet area, the inlet velocity is increased (decreased) to maintain the same mass flow rate, which can also induce pressure drop change. Moreover, the staggered distribution of ribs can also induce larger pressure, just like pressure drop increase in channel with obstacles [36-37], for which higher pressure is needed to impel gas flow to transfer forward.

Considering the average current density deviation between all the cases lies within 27% and the maximum temperature difference between all the cases only differs slightly (within 2 K), the pressure drop difference induced by viscosity can be ignored here. The major factors inducing larger or smaller pressure drop for case 2-case 8 than that of case 1 have been illustrated in Table 4. It can be seen from table 4, case 3 has the largest pressure drop, because the discrete ribs act as obstacles for gas flow and the interval between ribs is narrow. Case 7 has a smaller pressure drop than case 1, because the equivalent hydraulic diameter increases along air flow.

Table 4 Pressure drop change and possible reasons

Cases	P_{in}-P_{out}	Possible reasons for increase or decrease of pressure drop
Case 1	5 Pa	
Case 2	11 Pa	Longer flow path, increased u, decreased D
Case 3	22 Pa	Longer flow path, decrease D
Case 4	21 Pa	Longer flow path, decreased D
Case 5	10 Pa	Decreased D
Case 6	14 Pa	Longer flow path, decreased D
Case 7	4 Pa	Increased D
Case 8	10 Pa	Longer flow path

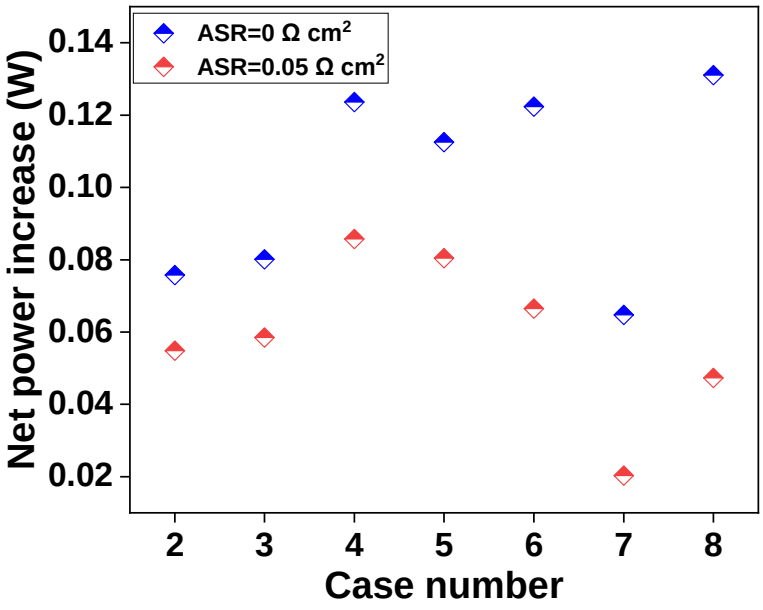

Fig. 7 Net power gain

Even though the larger inlet pressure increases the parasitic power loss, compared with the increased electrical power by using new IC, the parasitic power loss can be neglected. For example, when ASR is not considered, the output power of case 4 has increased by 0.12 W than that of traditional SOFC. However, the parasitic power increase is only 4.8E-5 W, only 0.04% of the increased electrical power. For each case with and without considering ASR, the parasitic power increase occupies less than 0.1% of the increased electric power as calculated. Compared to case 1, the net power gains of the other cases are displayed in Fig. 7. As seen, the net power gains of all the cases are positive. Consequently, the newly proposed IC designs are excellent alternatives to traditional IC in perspective of net power gain when ASR is not considered. When ASR is considered, all the cases except for case 7 have obvious net power gain than that of case 1, while case 7 has relatively slight net power advantage over case 1 when ASR is considered.

4. Conclusions

The multi-physics model is built to numerically investigate the effect of IC design on the performance of SOFC. Discrete rib designs (case 2 and case 3), staggered rhombus rib design (case 4), narrowed rib design (case 5), continuous wave-like rib design (case 6), trapezoid IC design (case 7), and the staggered cuboid rib design (case 8) are proposed to study the influence of IC design on the performance of SOFC. The unconventional IC designs proposed in this study improve the performance of SOFC dramatically in the perspective of long-term stable high electrical power output and peak power density. The main conclusions include:

(1) Case 8 performs best when ASR is not considered, while case 4 behaves best when ASR increases to 0.05 Ω cm^2. In the two conditions, case 5 and case 6 have obvious superiority, and case 2 and case 3 can also improve the performance of SOFC significantly. Case 7 has relatively commonplace advantage of output power when IC is not oxidized, while this advantage is greatly weakened when contact resistance is increased to 0.05 Ω cm^2.

(2) The rib size, spatial layout of discrete ribs, contact resistance and the IC/electrode contact area are key factors affecting the electrical performance of SOFC. The performance improvement of SOFC by using new IC designs can be attributed to the shortened current collection path, decreased gas transfer path in cathode or increased residual time for air flow in channels.

(3) Considering the long-term performance degradation induced by IC oxidation, the performance of newly designed SOFC with smaller IC/electrode contact area tends to degrade more seriously. It also revealed that the parasitic power increase occupies less than 0.1% of the increased power output, therefor it can be neglected.

(4) SOFC with all the newly designed ICs can keep long-term higher net power output than the traditionally designed SOFC. However, the performance of case 2 and 3 can be further improved by optimizing the size of rib and the interval between ribs. The performance of case 6 and 8 can be further optimized by increasing the contact area.

Acknowledgement

This work was supported by the Project of Strategic Importance funding scheme (Project ID: P0035168) from The Hong Kong Polytechnic University.

References

[1] Kornely, M., Leonide, A., Weber, A. & Ivers-Tiffée, E. Performance limiting factors in anode-supported cells originating from metallic interconnector design. J. Power Sources 2011; 196:7209-7216.

[2] Guan, W. & Wang, W. G. Electrochemical Performance of Planar Solid Oxide Fuel Cell (SOFC) Stacks: From Repeat Unit to Module. Energy Technology 2014; 2:692-697.

[3] Gazzarri, J. I. & Kesler, O. Short-stack modeling of degradation in solid oxide fuel cells. Part I. Contact degradation. J. Power Sources 2008; 176:138-154.

[4] Jiang, S. P., Love, J. G. & Apateanu, L. Effect of contact between electrode and current collector on the performance of solid oxide fuel cells. Solid State Ionics 2003; 160:15-26.

[5] Zhu, J. & Lin, Z. Degradations of the electrochemical performance of solid oxide fuel cell induced by material microstructure evolutions. Appl. Energy 2018; 231:22-28.

[6] Nishida, R., Beale, S., Pharoah, J., de Haart, L. & Blum, L. Three-dimensional computational fluid dynamics modelling and experimental validation of the Jülich Mark-F solid oxide fuel cell stack. J. Power Sources 2018; 373:203-210.

[7] Lin, Z., Stevenson, J. W. & Khaleel, M. A. The effect of interconnect rib size on the fuel cell concentration polarization in planar SOFCs. J. Power Sources 2003; 117:92-97.

[8] Jeon, D. H., Nam, J. H. & Kim, C.-J. Microstructural Optimization of Anode-Supported Solid Oxide Fuel Cells by a Comprehensive Microscale Model. J. Electrochem. Soc 2006; 153: A406.

[9] Kong, W., Li, J., Liu, S. & Lin, Z. The influence of interconnect ribs on the performance of planar solid oxide fuel cell and formulae for optimal rib sizes. J. Power Sources 2012; 204:106-115.

[10] Liu, S., Kong, W. & Lin, Z. Three-dimensional modeling of planar solid oxide fuel cells and the rib design optimization. J. Power Sources 2009; 194:854-863.

[11] Zhan R, Wang Y, Ni M, Zhang G, Du Q & Jiao K. Three-dimensional simulation of solid oxide fuel cell with metal foam as cathode flow distributor. Int. J. Hydrogen Energy 2020; 45:6897–911.

[12] Timurkutluk B, Ucar E. Development of high performance and low-cost solid oxide fuel cell stacks: Numerical optimization of flow channel geometry. Int. J. Energy Res 2021; 1–17.

[13] Awin, Y., & Dukhan, N. Experimental performance assessment of metal-foam flow fields for proton exchange membrane fuel cells. Appl. Energy 2019; 252:113458.

[14] Atyabi, S. A., & Afshari, E. Three-dimensional multiphase model of proton exchange membrane fuel cell with honeycomb flow field at the cathode side. J. Cleaner Production 2019; 214:738-748.

[15] Wang, Y., Si, C., Qin, Y., Wang, X., Fan, Y., & Gao, Y. Bio-inspired design of an auxiliary fishbone-shaped cathode flow field pattern for polymer electrolyte membrane fuel cells. Energy Convers. Manag 2021; 227:113588.

[16] Jang, J. Y., Cheng, C. H., Liao, W. T., Huang, Y. X., & Tsai, Y. C. Experimental and numerical study of proton exchange membrane fuel cell with spiral flow channels. Appl. Energy 2012; 99:67-79.

[17] Damian-Ascencio, C. E., Saldaña-Robles, A., Hernandez-Guerrero, A., & Cano-Andrade, S. Numerical modeling of a proton exchange membrane fuel cell with tree-like flow field channels based on an entropy generation analysis. Energy 2017; 133:306-316.

[18] Gao, X., Zhang, Q., Zhang, W. & Chen, D. Optimization of distributed cylindrical interconnect ribs for anode- and cathode-supported solid oxide fuel cell. Int. J. Electrochem. Sci 2015; 10:7521-7534.

[19] Kong, W., Han, Z., Lu, S., Gao, X., & Wang, X. A novel interconnector design of SOFC. Int. J. Hydrogen Energy 2020; 45: 20329-20338.

[20] Fu, Q., Li, Z., Wei, W., Liu, F., Xu, X. & Liu, Z. Performance enhancement of a beam and slot interconnector for anode-supported SOFC stack. Energy Convers. Manag 2021; 241:114277.

[21] Bhattacharya, D., Mukhopadhyay, J., Biswas, N., Basu, R. N. & Das, P. K. Performance evaluation of different bipolar plate designs of 3D planar anode-supported SOFCs. Int. J. Heat Mass Transf 2018; 123:382-396.

[22] Zhao, F., & Virkar, A. V. Dependence of polarization in anode-supported solid oxide fuel cells on various cell parameters. J. Power Sources 2005; 141:79-95.

[23] Suwanwarangkul, R., Croiset, E., Fowler, M. W., Douglas, P. L., Entchev, E. & Douglas, M. A. Performance comparison of Fick's, dusty-gas and Stefan-Maxwell models to predict the concentration overpotential of a SOFC anode. J. Power Sources 2003; 122:9-18.

[24] Chen, D., Lin, Z., Zhu, H., & Kee, R. J. Percolation theory to predict effective properties of solid oxide fuel-cell composite electrodes. J. Power Sources 2009; 191: 240-252.

[25] Guo M, Xiao G, Wang J qiang. & Lin Z. Parametric study of kW-class solid oxide fuel cell stacks fueled by hydrogen and methane with fully multiphysical coupling model. Int. J. Hydrogen Energy 2021; 46:9488–502.

[26] Liu H, Li P, Juarez-Robles D, Wang K. & Hernandez-Guerrero A. Experimental study and comparison of various designs of gas flow fields to PEM fuel cells and cell stack performance. Front Energy Res 2014; 2:1–8.

[27] Liu H, Li P, Juarez-Robles D, Wang K. & Hernandez-Guerrero A. Experimental study and comparison of various designs of gas flow fields to PEM fuel cells and cell stack performance. Front Energy Res 2014; 2:1–8.

[28] Noh, H. S., Hwang, J., Yoon, K., Kim, B. K., Lee, H. W., Lee, J. H. & Son, J. W. Optimization of current collection to reduce the lateral conduction loss of thin-film-processed cathodes. J. Power Sources 2013; 230:109-114.

[29] Talic B, Falk-Windisch H, Venkatachalam V, Hendriksen PV, Wiik K. & Lein HL. Effect of coating density on oxidation resistance and Cr vaporization from solid oxide fuel cell interconnects. J. Power Sources 2017; 354:57–67.

[30] Brylewski T, Kruk A, Bobruk M, Adamczyk A, Partyka J. & Rutkowski P. Structure and electrical properties of Cu-doped Mn-Co-O spinel prepared via soft chemistry and its application in intermediate-temperature solid oxide fuel cell interconnects. J. Power Sources 2016; 333:145–55.

[31] Zhu WZ. & Deevi SC. Opportunity of metallic interconnects for solid oxide fuel cells: A status on contact resistance. Mater Res Bull 2003; 38:957–72.

[32] Liu, S., Song, C. & Lin, Z. The effects of the interconnect rib contact resistance on the performance of planar solid oxide fuel cell stack and the rib design optimization. J. Power Sources 2008; 183:214-225.

[33] Tu H, Stimming U. Advances, aging mechanisms and lifetime in solid-oxide fuel cells. J.Power Sources 2004; 127:284–93.

[34] Wang, J. Theory and practice of flow field designs for fuel cell scaling-up: A critical review. Appl. Energy 2015; 157:640–663.

[35] Saied, M., Ahmed, K., Nemat-Alla, M., Ahmed, M. & El-Sebaie, M. Performance study of solid oxide fuel cell with various flow field designs: numerical study. Int. J. Hydrogen Energy 2018; 43:20931–20946.

[36] Bilgili M, Bosomoiu M. & Tsotridis G. Gas flow field with obstacles for PEM fuel cells at different operating conditions. Int. J. Hydrogen Energy 2015; 40:2303–11.

[37] Heidary H, Kermani MJ, Advani SG. & Prasad AK. Experimental investigation of in-line and staggered blockages in parallel flow field channels of PEM fuel cells. Int. J. Hydrogen Energy 2016; 41:6885–93.